Boosting Spin-Orbit-Torque Efficiency in Spin-Current-Generator/Magnet/Oxide Superlattices

Lijun Zhu,[1,2,*] Jingwei Li,[3] Lujun Zhu,[4] and Xinyue Xie[4]

[1] *State Key Laboratory of Superlattices and Microstructures, Institute of Semiconductors, Chinese Academy of Sciences, Beijing 100083, China*

[2] *College of Materials Science and Opto-Electronic Technology, University of Chinese Academy of Sciences, Beijing 100049, China*

[3] *Multi-scale Porous Materials Center, Institute of Advanced Interdisciplinary Studies & School of Chemistry and Chemical Engineering, Chongqing University, Chongqing 400044, China*

[4] *College of Physics and Information Technology, Shaanxi Normal University, Xi'an 710062, China*

(Received 17 May 2022; revised 13 October 2022; accepted 16 November 2022; published 16 December 2022)

Efficient manipulation of magnetic materials is essential for spintronics. In conventional spin-current-generator/magnet (SCG/M) bilayers, interfacial spin-orbit torques (SOTs) lose effectiveness in applications that require large magnetic layer thicknesses to maintain magnetic anisotropy and stability at lateral sizes of tens of nanometers (e.g., magnetic tunnel junctions and racetrack nanowires). Here, we develop a universally workable three-dimensional spin-orbit material scheme in which the SOT efficiency can be remarkably boosted towards infinity by stacking [SCG/M/oxide]$_n$ superlattices, with the oxide layers breaking inversion symmetry. We demonstrate that this superlattice scheme promotes not only perpendicular magnetic anisotropy for an effectively rather thick magnetic layer but also enables switching of such thick magnetic layers by interfacial SOTs with n^2 times lower power consumption than the corresponding conventional bilayer scheme with the same total thicknesses for the SCG and M. In contrast, we find that spin torque diminishes in second-type superlattices, [SCG/M]$_n$, lacking inversion-symmetry breaking. These results provide an in-depth understanding of SOTs in magnetic multilayers and establish [SCG/M/oxide]$_n$ superlattices as advantageous building blocks for the development of low-power, high-stability, and high-endurance spintronic memory and computing.

DOI: 10.1103/PhysRevApplied.18.064052

I. INTRODUCTION

Strong spin-orbit torques (SOTs) [1,2] have promise to enable fast low-power magnetization manipulation in magnetic memory and computing technologies. In the simple case of a bilayer consisting of a spin-current generator (SCG) and a magnetic layer (M) [Fig. 1(a)], a transversely polarized spin current generated by the SCG diffuses into M and exerts interfacial SOTs on magnetization. When the spin Hall effect (SHE) is the dominant source of the spin current (as in the case of heavy metals [2–4], Bi-Sb [5,6], Bi_xTe_{1-x} [7], Co_xPt_{1-x} [8], Fe_xTb_{1-x} [9], Co-Ni-B [10], $SrIrO_3$ [11], etc.) and when the spin current relaxes within the magnetic layer via dephasing, the dampinglike SOT efficiency per current density (ξ^j_{DL}) is given by $\xi^j_{DL} \approx T_{int}\theta_{SH}$. Here, the internal spin Hall ratio (θ_{SH}) of the SCG is the product of the resistivity (ρ_{xx}) and the spin Hall conductivity (σ_{SH}), i.e., $\theta_{SH}=\sigma_{SH}\rho_{xx}$; T_{int} is the spin transparency of the interface, which determines what fraction of the spin current enters the magnet.

In such conventional bilayers, ξ^j_{DL} is usually low, particularly when θ_{SH} is small and when T_{int} is far less than unity due to spin memory loss [12–18] and spin backflow [19–23] (e.g., $\xi^j_{DL} \approx 0.05-0.15$ for Pt/3d ferromagnet [3]). A more critical limitation of the bilayer scheme is that the efficiency of the dampinglike SOT per magnetic layer thickness (t), ξ^j_{DL}/t, is inversely proportional to t. This degrades the effectiveness of the interfacial SOTs in spintronic applications where M has to be thick to maintain a bulk [9,24] or shape [25,26] perpendicular magnetic anisotropy (PMA) and/or thermal stability when the lateral size scales down to tens of nanometers (e.g., magnetic tunnel junctions and racetrack nanowires).

The main idea of this work is to "accumulate" ξ^j_{DL} by stacking of the SCG/M/oxide superlattice. Here, the SCG generates spin current that diffuses into the adjacent M, and the oxide breaks the inversion symmetry for a total torque to occur. In the SCG/M/oxide superlattice

*ljzhu@semi.ac.cn

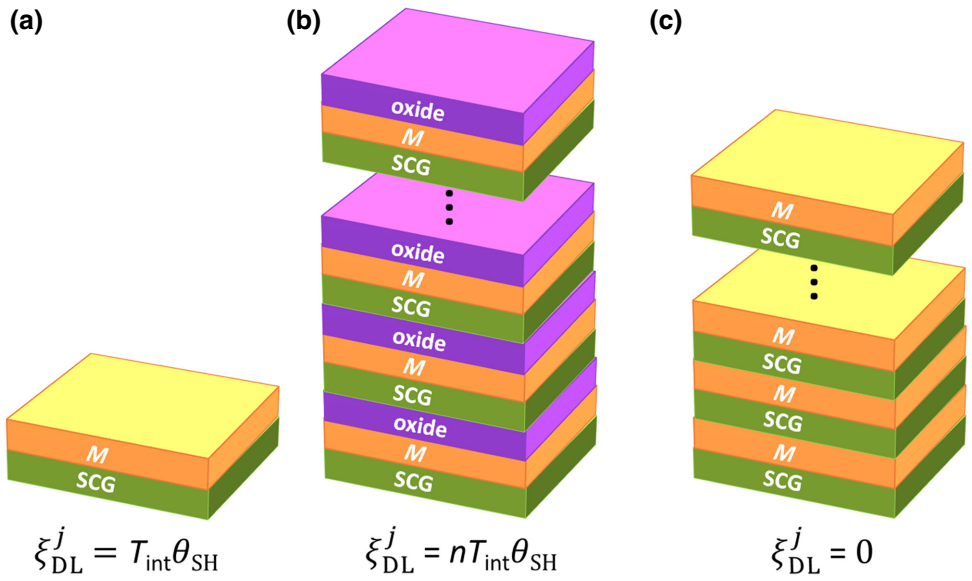

FIG. 1. Dampinglike spin-orbit-torque efficiency expected for three material schemes: (a) SCG/M bilayer, (b) [SCG/M/oxide]$_n$ superlattice, (c) [SCG/M]$_n$/SCG superlattice.

[Fig. 1(b)], the dampinglike efficiency would be enhanced by a factor of the repeat number n, i.e., $\xi^j_{DL} = nT_{int}\theta_{SH}$, if all repeats were identical and the thickness of the M were greater than the spin-dephasing length (l_{DP}). When n is infinite, the spin-orbit torque would, in principle, also diverge. Any bulk SOT generated within the M layer is ignored in this model because bulk SOT is significant at the bulk limit but vanishes at the small thicknesses [8,9] necessary for the superlattice scheme. However, in the [SCG/M]$_n$/SCG superlattice with no symmetry-breaking oxide layer [Fig. 1(c)], no torque is expected due to cancellation of the spin currents from the two SCG layers sandwiching M. Here, we experimentally verify that ξ^j_{DL} is remarkably boosted in the SCG/M/oxide superlattice, using the prototype SCG Pt, 3d Co, and MgO, and that the SOT diminishes in Pt/Co superlattice.

II. SAMPLE DETAILS

For this work, we sputter-deposit Pt(2)/Co(0.8)/MgO(2), [Pt(2)/Co(0.8)/MgO(2)]$_5$, [Pt(2)/Co(0.8)/MgO(2)]$_{10}$, Pt(20)/Co(0.8)/MgO(2), Pt(2)/Co(0.8)/Pt(2), [Pt(2)/Co(0.8)]$_5$, and [Pt(2)/Co(0.8)]$_{10}$ (here, the numbers in parentheses following the materials are layer thicknesses in nm and the subscripts represent the repeat number). Each sample is deposited on an oxidized Si substrate with a 1-nm Ta seed layer and capped by a 2-nm MgO layer and a 1.5-nm Ta layer that is oxidized upon exposure to the atmosphere. The Ta seed layer is very resistive and contributes negligible spin current to other layers. The layer thicknesses are estimated using the calibrated deposition rates and the deposition time. A thickness of 0.8 nm is chosen for the Co layers as a compromise between the interfacial PMA and spin dephasing within Co. For electrical measurements, the samples are patterned into 5 × 60 μm^2 Hall bars [Fig. 2(a)] by photolithography and ion milling. No annealing is performed on the samples.

As measured by a superconducting quantum interference device using unpatterned sample pieces that undergo the same lithography and ion-milling processes as the Hall bars, the average saturation magnetization (M_s) of the thin Co layers is 790–1470 emu/cm^3 **(**see Fig. 2(b) for the example of [Pt(2)/Co(0.8)/MgO(2)]$_{10}$**)**. M_s is 1275–1425 emu/cm^3 for Pt(2)/Co(0.8)/Pt(2), [Pt(2)/Co(0.8)]$_5$, and [Pt(2)/Co(0.8)]$_{10}$. The magnetization variation of the 0.8-nm Co layers is likely to be due to different degrees of the magnetic proximity effect [27] at the Co/Pt and Pt/Co interfaces and reduction of the Curie temperature for thin Co induced by the roughness (see below), but these M_s values are within the range of literature values [27–31]. Apart from in-plane magnetized Pt(2)/Co(0.8)/MgO(2), all the other samples show good PMA, as indicated by the in-plane saturation field, H_k [Fig. 2(b)], and by the out-of-plane field-dependent Hall resistance hysteresis [Fig. 2(c)].

III. ENHANCEMENT OF SOT IN SCG/M/OXIDE SUPERLATTICES

To determine the SOTs, we perform harmonic Hall voltage response (HHVR) measurements [9,32–34] by carefully taking into account thermoelectric effects. To determine the current-driven dampinglike SOT field (H_{DL}) for the PMA samples, the first and second HHVRs, V_ω and $V_{2\omega}$, respectively, are collected as a function of the

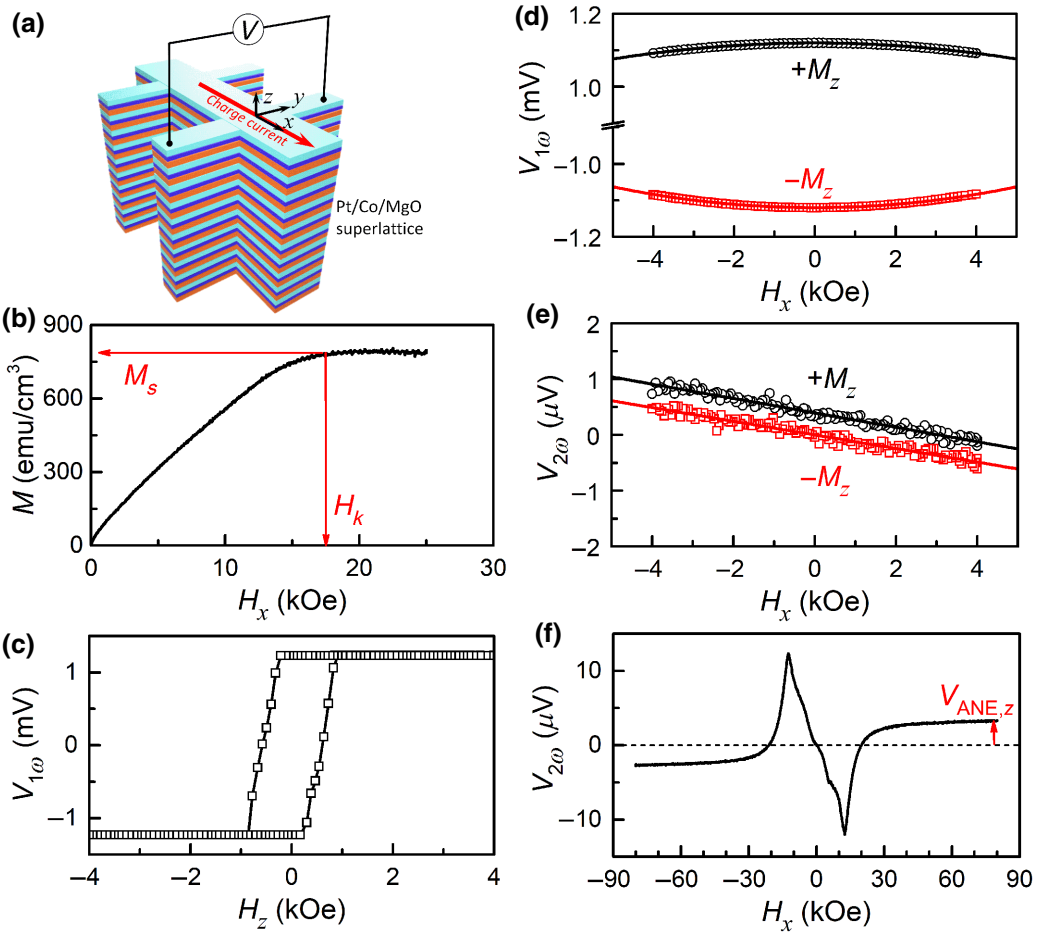

FIG. 2. (a) Schematic of the Pt/Co/MgO superlattice. (b) In-plane magnetization versus in-plane magnetic field (H_x). (c) First-harmonic Hall voltage ($V_{1\omega}$) versus out-of-plane magnetic field (H_z); (d) $V_{1\omega}$ versus H_x. (e) Second-harmonic Hall voltage ($V_{2\omega}$) versus H_x, and (f) $V_{2\omega}$ versus H_x for the $[Pt(2)/Co(0.8)/MgO(2)]_{10}$ superlattice. Red arrows in (b) indicate saturation magnetization and the perpendicular magnetic anisotropy field. Data in (d),(e) are collected by first saturating magnetization along the film normal (i.e., $\pm M_z$) under an out-of-plane magnetic field and then sweeping H_x in the range well below H_k of the sample, so that magnetization is tilted in a small range and following the macrospin model. In (f), data are collected by sweeping H_x between -80 and 80 kOe ($\gg H_k$), and red arrow indicates the anomalous Nernst voltage induced by the perpendicular thermal gradient.

small in-plane field, H_x ($\ll H_k$), swept along the current direction, under the applied sinusoidal electric field with a magnitude of $E = 33.3$ kV/m. In this case, V_ω and $V_{2\omega}$ are parabolic and linear functions of H_x **(**see Figs. 2(d) and 2(e) for $[Pt(2)/Co(0.8)/MgO(2)]_{10}$ and Fig. 6 in the Appendix A for the $[Pt(2)/Co(0.8)/MgO(2)]_5$**)**, i.e.,

$$V_\omega \approx V_{\mathrm{AHE}}(1 - {H_x}^2/2{H_k}^2), \tag{1}$$

$$V_{2\omega} = \frac{1}{2}\frac{V_{\mathrm{AHE}}}{H_k^2}H_{\mathrm{DL}}H_x + \frac{V_{\mathrm{ANE},z}}{H_k}H_x + V_{\mathrm{ANE},x}, \tag{2}$$

where V_{AHE} is the anomalous Hall voltage; $V_{\mathrm{ANE},x}$ and $V_{\mathrm{ANE},z}$ are the anomalous Nernst voltages due to the longitudinal and perpendicular thermal gradients, respectively. Note that $V_{2\omega}$ contains contributions that are proportional to H_x from both the dampinglike torque and the perpendicular thermal gradient. Combining Eqs. (1) and (2), one obtains

$$H_{\mathrm{DL}} = -2\frac{\partial V_{2\omega}}{\partial H_x}\Big/\frac{\partial^2 V_\omega}{\partial {H_x}^2} - 2H_k\frac{V_{\mathrm{ANE},z}}{V_{\mathrm{AHE}}}. \tag{3}$$

Here, $V_{\mathrm{ANE},z}$ is equal to the value of $V_{2\omega}$ when magnetization is fully aligned along the current direction by H_x that is greater than H_k [Fig. 2(f)]. Note that the value of H_{DL} cannot be separated from a linear scaling of $-2\frac{\partial V_{2\omega}}{\partial H_x}/\frac{\partial^2 V_\omega}{\partial {H_x}^2}$ with E. This suggests that the anomalous Nernst effect should be taken into account in the analysis of resistive magnetic systems with a small SOT field and a large H_k. The so-called "planar Hall correction" [35–39] is not applied in the out-of-plane HHVR analysis given the fact that neglecting the "correction" for the PMA samples in the

out-of-plane HHVR analysis gives results that are in close accordance with the in-plane HHVR results [36,40,41] and the results from measurements that do not involve the planar Hall effect (such as optical Sagnac interferometry [37], loop shift, and switching of in-plane spin-orbit-torque magnetic tunnel junctions [4]). As experimentally known for nearly a decade [35–39], the planar Hall correction, if significant, causes large errors for different material systems (see the Appendix B for details). However, since the $V_{\mathrm{PHE}}/V_{\mathrm{AHE}}$ ratio for samples in this work is 0.13–0.23, the planar Hall correction, if applied, can only change the values of H_{DL} and torque efficiencies by less than 20% and will not affect our conclusion. H_{DL} for the in-plane sample Pt(2)/Co(0.8)/MgO(2) is determined from angle-dependent in-plane HHVR measurements [36], which also take into account any thermoelectric effects (see Fig. 7 in the Appendix A).

With the H_{DL} values, the SOT efficiency per current density is calculated as

$$\xi^{j}_{\mathrm{DL}} = (2e/\hbar) M_s t H_{\mathrm{DL}}/j_c, \tag{4}$$

where e is elementary charge, $\hbar$ is the reduced Plank's constant, $j_c = E/\rho_{xx}$ is the current density in the Pt layer, and t is the total thickness of the magnetic layer and increases with the repeat number of the superlattice (i.e., t is n times the M thickness of each repeat). Strikingly, ξ^{j}_{DL} is enhanced from 0.15 for Pt(2)/Co(0.8)/MgO(2) to 0.27 for the five-repeat superlattice, $[\mathrm{Pt(2)/Co(0.8)/MgO(2)}]_5$, and to 0.57 for the ten-repeat superlattice, $[\mathrm{Pt(2)/Co(0.8)/MgO(2)}]_{10}$. ξ^{j}_{DL} for $[\mathrm{Pt(2)/Co(0.8)/MgO(2)}]_{10}$ is enhanced by a factor of about 4 compared to those for Pt(2)/Co(0.8)/MgO and Pt(20)/Co(0.8)/MgO(2) ($\xi^{j}_{\mathrm{DL}} \approx 0.14$). The giant value of ξ^{j}_{DL} for $[\mathrm{Pt(2)/Co(0.8)/MgO(2)}]_{10}$ is also greater than the spin Hall ratio of 0.5 for Pt at a resistivity of 30 μΩ cm [4]. This suggests that the SCG/M/oxide superlattice is a very effective spin-orbit material scheme to boost the total dampinglike SOT efficiency. Such enhancement cannot be attributed to the increase of the effective thickness of the Pt because we measure only a small ξ^{j}_{DL} of 0.14 for Pt(20)/Co(0.8)/MgO(2), which has the same total thickness of Pt and a high magnetization of 1470 emu/cm^3. [We also measure an in-plane sample, Pt(20)/Co(8)/MgO(2), but the strong contribution of the Oersted field overwhelms $V_{2\omega}$ and prevents accurate determination of ξ^{j}_{DL}.] Such enhancement of ξ^{j}_{DL} is unrelated to any spin-current generation by the Rashba effect or spin-orbit coupling at the interfaces because we measure negligible SOT at the SCG/FM [38] and FM/MgO interfaces [8,16], at least in our samples.

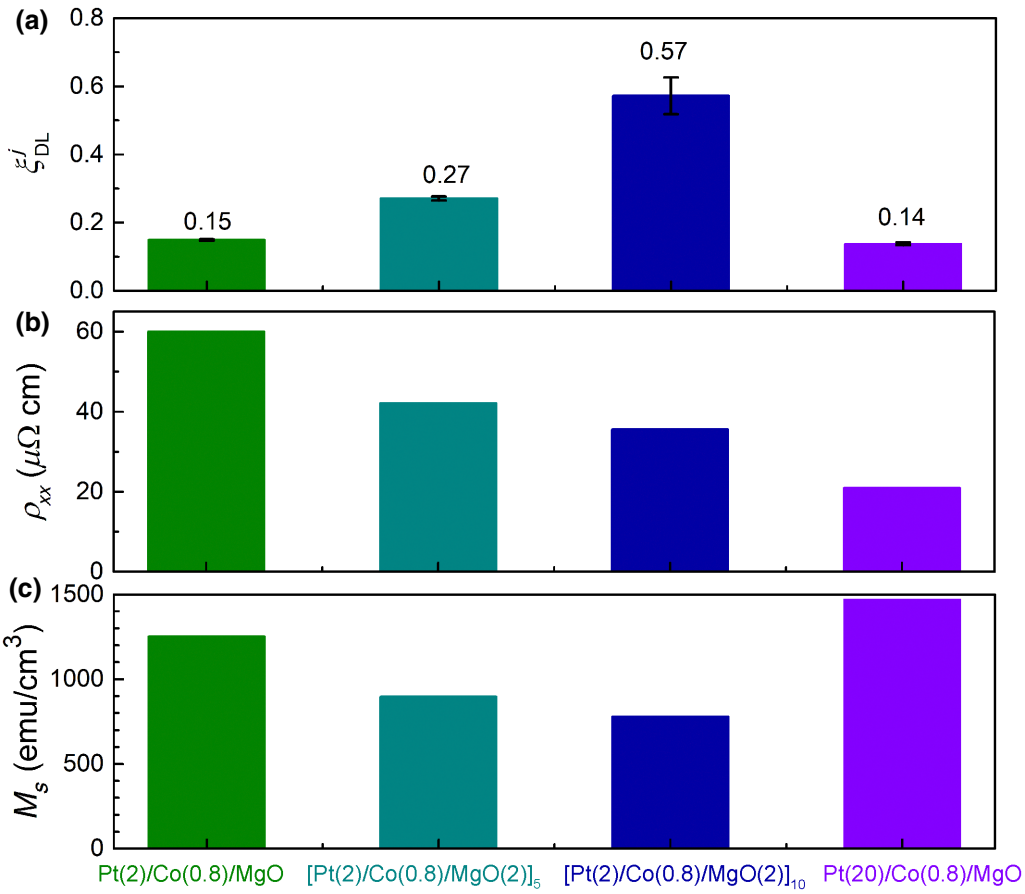

FIG. 3. (a) Dampinglike SOT efficiency, (b) resistivity, and (c) saturation magnetization for Pt(2)/Co(0.8)/MgO, $[\mathrm{Pt(2)/Co(0.8)/MgO(2)}]_5$, $[\mathrm{Pt(2)/Co(0.8)/MgO(2)}]_{10}$, and Pt(20)/Co(0.8)/MgO.

However, the "accumulation" rate of the SOT efficiency in the $[Pt/Co/MgO]_n$ superlattice in the present work appears to be slower than expected from the stacking of identical repeats. This suggests that the torque contribution of the Pt/Co/MgO repeats varies, with the bottom Pt/Co/MgO repeat grown on the 1-nm Ta adhesion layer contributing the largest torque efficiency (≈0.15). First, we find that the average ρ_{xx} for the Pt layers reduces from 60 μΩ cm for $n = 1$ to 35 μΩ cm for $n = 10$ [Fig. 3(b)]. Here, ρ_{xx} is estimated from the electrical conductance enhancement of the Pt/Co/MgO repeats relative to n times the conductance of a control sample, Ta(1)/Co(0.8)/MgO(2). The resistivity reduction in the Pt layers suggests approximately a factor of 2 reduction in the average spin Hall ratio of a single Pt/Co/MgO repeat because the intrinsic SHE of Pt predicts $\theta_{SH} = \sigma_{SH}\rho_{xx}$ [4]. Furthermore, the spin transparency of the Pt/Co interfaces should also decrease slightly with the repeat number due to the slowly decreasing ρ_{xx}. Within the Elliot-Yafet mechanism [42,43], a reduction of resistivity leads to an increase in the spin-diffusion length of Pt, and thus, spin backflow [4,19–23] at the Pt/Co interfaces. Note that spin memory loss [12–16] that arises from interfacial spin-orbit coupling is negligible at each Pt(2)/Co(0.8) interface in this work because we measure a small interfacial PMA energy density (K_s) that corresponds to negligible spin memory loss [16]. It is also well established that, at an interface with very weak SOC, the spin memory loss is not expected if the interface is sharp [12–14,16] or intermixed [44]. Within the Bruno model [45–48], interfacial spin-orbit coupling closely scales with K_s at interfaces with a relatively weak interfacial SOC and/or a relatively weak *d-d* orbital hybridization (such as Pt/Co interfaces [45]).

In addition, variation of the torque contribution of a single repeat may also be related to shortening of l_{DP} of Co for large repeat numbers. When l_{DP} is greater than the layer thickness of M, the spin current entering M from Pt cannot fully relax before getting reflected at the oxide interface. Polarization of the reflected spin current is usually rotated relative to the incident spin current [49,50], leading to reduction of the total torque. As shown in Fig. 3(c), the average saturation magnetization for the $[Pt(2)/Co(0.8)/MgO(2)]_n$ superlattice reduces from 1250 emu/cm^3 for $n = 1$ to 900 emu/cm^3 for $n = 5$ and 780 emu/cm^3 for $n = 10$. This would suggest a significant reduction in the average l_{DP} of Co with increasing n, if we assume that the l_{DP} of Co scales inversely with M_s. The evolution of the average Co magnetization with the repeat number seems to be related to the reduction of the smoothness of the Pt/Co/MgO repeat. As indicated by the cross-section scanning transmission electron microscopy image of the $[Pt(2)/Co(0.8)/MgO(2)]_{10}$ sample in Fig. 4, the Pt/Co/MgO repeat is fairly smooth for $n = 1$ but gets increasingly rough as n increases towards 10. We speculate that the increased roughness could lower the Curie temperature of the thin 0.8-nm Co layer, and thus, room-temperature magnetization.

While the exact cause of the resistivity and magnetization reduction needs further study, ξ^j_{DL} of a SCG/M/oxide superlattice can likely be optimized to increase in proportion to the repeat number, if the repeats can be kept identical through an improved growth protocol. Alternatively,

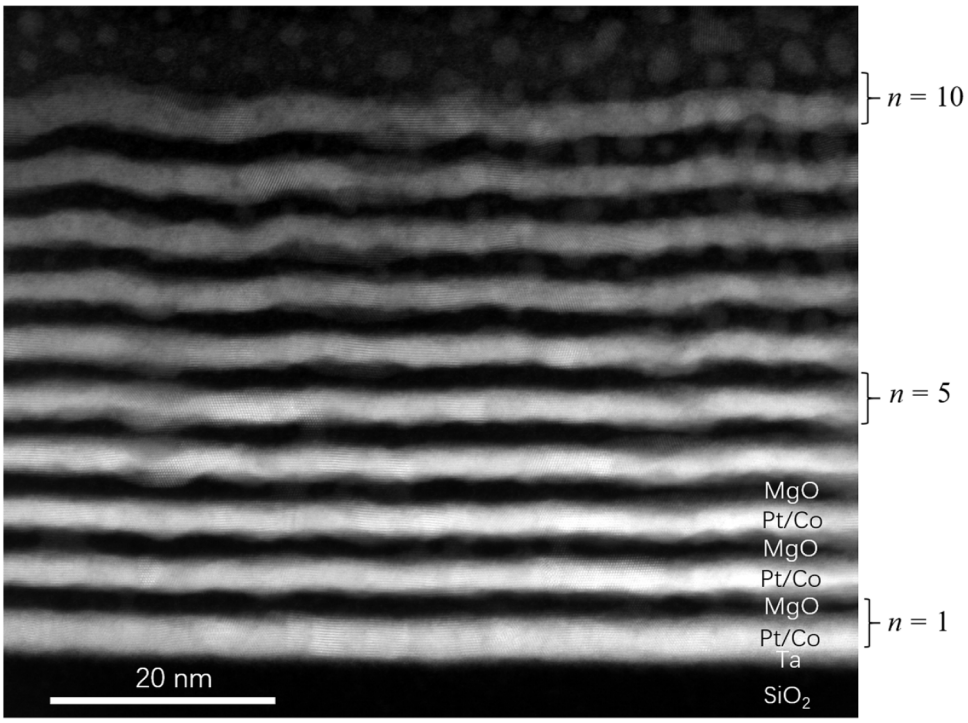

FIG. 4. Dark-field cross-section scanning transmission electron microscopy image for the $[Pt(2)/Co(0.8)/MgO(2)]_{10}$ superlattice, clearly indicating reduction of smoothness with increasing repeat number, n.

this might also be made possible if Pt and Co are replaced by a short mean-free-path SCG [e.g., $Au_{0.25}Pt_{0.75}$ [40] or $Pt_{0.7}(MgO)_{0.3}$ [3]] and a magnetic layer with M_s that is relatively insensitive to adjacent layers (e.g., Fe-Co-B).

IV. ABSENCE OF SIGNIFICANT SOT IN SCG/*M* SUPERLATTICES

We also perform HHVR measurements on the Pt/Co multilayers with no MgO insertion to break the inversion symmetry. As shown in Table I, simple stacking of Pt/Co repeats yields only low SOT efficiency because of the canceling effect of the spin currents of the two surrounding Pt layers of Co. The nonzero SOT suggests that the Pt/Co and Co/Pt interfaces are not perfectly symmetric, with the top interface contributing a greater SOT. However, this asymmetry, even for ten repeats, can only contribute a SOT efficiency that is substantially weaker than that of simple Pt/Co bilayers. Our finding of minimal SOT in the Pt/Co superlattice is in sharp contrast to previous reports of giant SOTs in Co/Pd multilayers [29] and Pt/Co multilayers [28,30,31,51], but in those works the thermoelectric effect is overlooked. As we show in Table I, if the ANE is ignored for our samples, a "giant" value of apparent ξ^j_{DL} (such as 1.7 for $[Pt(2)/Co(0.8)]_{10}$) may also be concluded, which is, however, incorrect.

V. PRACTICAL IMPACT

Finally, we discuss the practical impact of the $[SCG/M/oxide]_n$ superlattice. We first demonstrate that the spin-orbit material scheme we develop here, a three-dimensional $[SCG/M/oxide]_n$ superlattice, makes it possible to switch rather thick 3*d* ferromagnets with strong perpendicular magnetic anisotropy. As shown in Fig. 5, the $[Pt(2)/Co(0.8)/MgO(2)]_n$ superlattice, which has a total Co thickness of 8 nm, a giant perpendicular anisotropy field of $H_k = 17.5$ kOe, a high coercivity of $H_c = 0.6$ kOe, and a moderate magnetization of $M_s = 780$ emu/cm^3, is deterministically switched by the SOT at a current density (j_{c0}) of about 2×10^7 A/cm^2 within Pt (the corresponding average current density is $\approx 1 \times 10^7$ A/cm^2 for the entire superlattice). This is in striking contrast to the conventional SCG/*M* bilayer scheme, for which a Co layer is unlikely to be switchable by interfacial SOT before blowout of the device due to Joule heating when the thickness is several nanometers, e.g., 8 nm, and can hardly maintain PMA when the effective thickness is above 1.5 nm. The ability of the superlattice to effectively switch a thick magnetic layer is interesting for spintronic applications, where *M* has to be thick to maintain PMA and/or thermal stability when the lateral size scales down to tens of nanometers.

TABLE I. Spin-orbit torque in Pt/Co multilayers, as determined from out-of-plane HHVR with and without taking into account the anomalous Nernst effect (ANE).

Materials	ρ_{xx} (μΩ cm)	ξ^j_{DL} (w/ANE)	ξ^j_{DL} (w/o ANE)
Pt(2)/Co(0.8)/Pt(2)	57	−0.03	−0.08
$[Pt(2)/Co(0.8)]_5$	37	-0.04 ± 0.01	-0.44 ± 0.01
$[Pt(2)/Co(0.8)]_{10}$	34	-0.05 ± 0.06	-1.71 ± 0.06

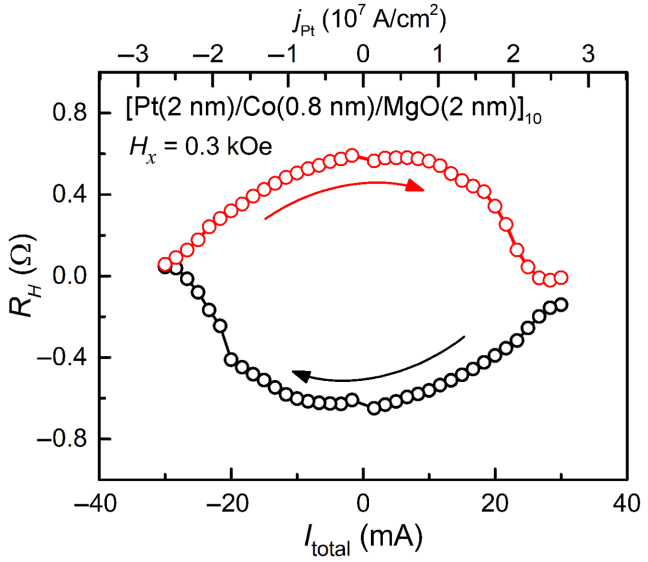

FIG. 5. Hall resistance of the $[Pt(2)/Co(0.8)/MgO(2)]_n$ superlattice versus total current and current density in the Pt layers, showing deterministic switching of perpendicular magnetic anisotropy of Co (total Co thickness = 8 nm, $H_k = 17.5$ kOe, $H_c = 0.6$ kOe, $M_s = 780$ emu/cm^3) by the spin-orbit torque at a current density of about 2×10^7 A/cm^2 within Pt (average current density of $\approx 1 \times 10^7$ A/cm^2 for the entire superlattice). In-plane bias field of 0.3 kOe is applied along the current direction to overcome the Dzyaloshinskii-Moriya interaction effect, such that the spin torque can take effect.

More quantitatively, the current density for switching 8-nm Co, in total, of the superlattice is just comparable to or even smaller than that of Pt/Co and Pt alloy/Co bilayers with a Co thickness of about 0.8 nm [52]. We also recently measured j_{c0} of 8.2×10^7 A/cm^2 for a Pt(2)/Co(1.4) bilayer (annealed to obtain PMA) [52], predicting 4.7×10^7 A/cm^2 for a Pt(2)/Co(0.8) bilayer, which is more than twofold higher than that for the $[Pt(2)/Co(0.8)/MgO(2)]_n$ superlattice. The current switching loop is gradual due to the distribution of the depinning field (switching field) during field switching [Fig. 2(c)] and is likely to be an effect of structural smoothness variation (Fig. 4). Here, we do not attempt to quantitatively estimate the value of ξ^j_{DL} by applying a macrospin or a domain-wall-motion model to current switching experiments because of a lack of simple correlation between the switching current density and ξ^j_{DL} of perpendicularly magnetized SCG/*M* heterostructures [52].

More generally, the superlattice has n times greater ξ^j_{DL}, and thus, n^2 times lower power consumption to generate a given spin-torque strength than the corresponding SCG/M bilayer with the same total thicknesses for SCG and M (assuming identical repeats for simplicity). Compared to a single SCG/M/MgO repeat, the superlattice has n times smaller impedance, which makes the superlattice have a factor of n reduced thermal degradation, and thus, improved device endurance. The superlattice also has enhanced perpendicular magnetic anisotropy (e.g., $[Pt(2)/Co(0.8)/MgO(2)]_n$ is in-plane magnetized for $n=1$ but perpendicularly magnetized for $n=5$ and 10), and thus, thermal stability compared to the single SCG/M bilayer. The superlattice also provides the possibility to flexibly tune the magnetic parameters (e.g., PMA and Dzyaloshinskii-Moriya interaction) via the layer thicknesses and repeat number. Therefore, such a SCG/M/oxide superlattice is a particularly advantageous spin-orbit material scheme for the development of energy-efficient high-density high-stability high-endurance spintronic memory and computing devices.

VI. SUMMARY

We develop a three-dimensional spin-orbit material scheme made by stacking of a spin-current-generator/magnet/oxide superlattice, in which the SOT efficiency can be remarkably boosted up to and even above the spin Hall ratio of the SCG. The superlattice scheme, $[SCG/M/oxide]_n$, can have enhanced perpendicular magnetic anisotropy, enhanced tunability, and n^2 times lower power consumption to generate a given spin-torque strength compared with the corresponding SCG/M bilayer with the same total thicknesses for the SCG and M. However, in the counterpart of the spin-current-generator/magnet superlattice with no symmetry-breaking oxide insertions, the SOT diminishes. The spin-current-generator/magnet/oxide material scheme, which we develop in this work, should universally work for superlattices with the SCG being a spin Hall metal (not limited to Pt), an orbital Hall metal, a topological insulator, and a complex oxide, and with the magnet being a ferromagnet, a ferrimagnet, or an antiferromagnet. This $[SCG/M/oxide]_n$ material scheme might also benefit from using self-torqued magnetic layers [8,9,53–58] as the M layer, if the bulk SOT can be engineered to be significant at small thicknesses (still a challenge) and additive to the interfacial SOT. These results not only advance the in-depth understanding of spin-orbit-torque physics in magnetic superlattices but also establish spin-current SCG/M/oxide superlattices as compelling building blocks for the development of energy-efficient high-endurance high-density SOT memory and computing technologies.

ACKNOWLEDGMENTS

This work is supported by the Strategic Priority Research Program of the Chinese Academy of Sciences (Grant No. XDB44000000) and by the National Natural Science Foundation of China (Grant No. 12274405).

APPENDIX A: ADDITIONAL SPIN-ORBIT TORQUE MEASUREMENT DATA

Figure 6 shows the out-of-plane HHVR results for the $[Pt(2)/Co(0.8)/MgO(2)]_5$ superlattices. The dampinglike-torque effective field, H_{DL}, of in-plane magnetized Pt(2)/Co(0.8)/MgO(2) are determined from in-plane HHVR measurements. As shown in Fig. 7(a), the second HHVR of an in-plane magnetization is given by

$$V_{2\omega} = (V_{DL} + V_{ANE,Z})\cos\varphi + V_{FL+Oe}\cos\varphi\cos 2\varphi, \tag{A1}$$

where $V_{DL} = -V_{AH}H_{DL}/2(H_{in} + |H_k|)$ is the second HHVR from the dampinglike SOT, V_{FL} is the second HHVR from the fieldlike SOT and Oersted field torque, $V_{ANE,Z}$ is the anomalous Nernst voltage, and H_{in} is the in-plane bias field. The slope of V_{DL} versus $-V_{AH}/2(H_{in} + |H_k|)$ yields the value of H_{DL} [Fig. 7(b)].

APPENDIX B: ABSENCE OF THE PLANAR HALL CORRECTION

Next we discuss the absence of the planar Hall correction. As suggested by Hayashi *et al.* in 2014 [34], the planar Hall effect appears to be involved in the out-of-plane

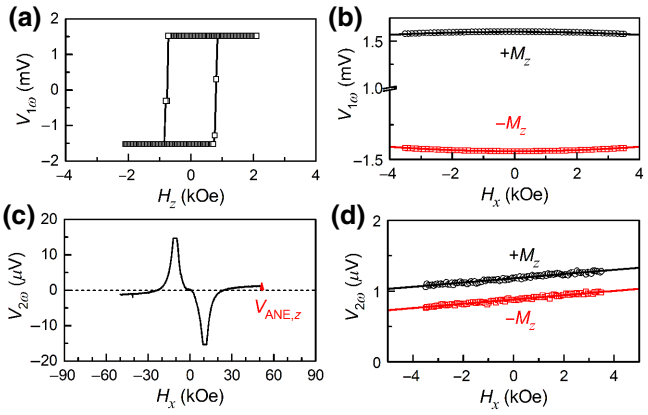

FIG. 6. Out-of-plane harmonic Hall voltage response measurement on the $[Pt(2)/Co(0.8)/MgO(2)]_5$ superlattice. (a) First-harmonic Hall voltage ($V_{1\omega}$) versus out-of-plane magnetic field (H_z), (b) $V_{1\omega}$ versus H_x. (c),(d) Second-harmonic Hall voltage ($V_{2\omega}$) versus H_x. Red arrow in (c) indicates the anomalous Nernst voltage induced by the perpendicular thermal gradient. Solid lines in (b),(d) represent fits of the data to Eqs. (1) and (2), respectively.

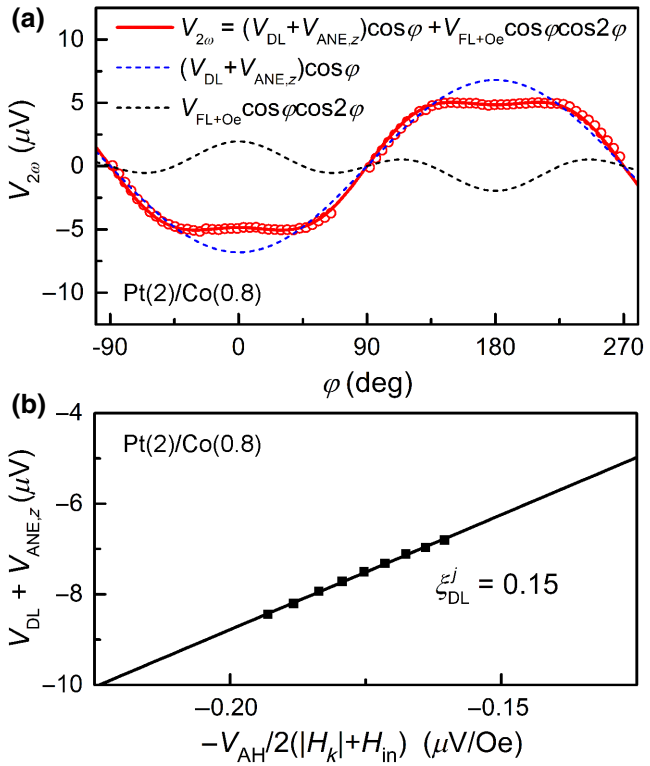

FIG. 7. (a) Second-harmonic Hall voltage response of in-plane magnetized Pt(2)/Co(0.8)/MgO(2). Red curve refers to the best fit of the data to Eq. (A1). (b) Linear fit of V_{DL} versus $-V_{AH}/2(H_{in}+|H_k|)$, the slope of which yields the value of H_{DL}. Applied electric field is 66.7 kV/m.

HHVR on samples with PMA and to modify the fieldlike and dampinglike spin-torque efficiencies as

$$\xi^j_{DL(FL)}(\text{with correction}) = (\xi^j_{DL(FL)} + 2\zeta\xi^j_{FL(DL)})/(1-4\zeta^2), \quad \text{(B1)}$$

where $\zeta = V_{PHE}/V_{AHE}$, and V_{PHE} and V_{AHE} are the planar Hall voltage and anomalous Hall voltage, respectively.

However, since the same year, 2014, this so-called planar Hall correction has been known by researchers, including the developer of this correction [35–39], to cause errors. First, this correction leads to infinite estimates for spin-orbit-torque efficiencies when $V_{PHE}/V_{AHE} = 0.5$ [see Eq. (A1)]. Experimentally, when V_{PH}/V_{AH} is very large, this correction leads to unrealistic magnitudes and even sign reversals for the extracted values of ξ^j_{DL}, with large discrepancies compared to other measurement methods (see Table II for examples of different material systems).

In contrast, *neglecting the correction for the PMA samples* in the out-of-plane HHVR measurements consistently gives results that are in close accordance with the in-plane HHVR results from in-plane magnetic anisotropy samples with the same heavy-metal/ferromagnet components and similar resistivities and thicknesses (see Table II, Fig. 8, and Refs. [36,40,41]) and with results from measurements that do not involve the planar Hall effect (such as optical Sagnac interferometry [37], domain-wall motion [35], loop shift, and switching of in-plane spin-orbit-torque magnetic tunnel junctions [4]). More discussions are reported in the Supplemental Material of Refs. [16,35,36]. Therefore, *it is experimentally clear that the so-called planar Hall correction should be avoided.*

Therefore, the planar Hall correction is not applied to the Pt/Co/MgO or Pt/Co superlattices in the main text (Fig. 3 and Table I). The physical mechanism for the absence of the planar Hall correction in the out-of-plane HHVR measurements is beyond the scope of our present work, because it is a long-standing open question for the whole spintronic community and because it is not specific to the superlattice samples in this work. We do note that, since the V_{PHE}/V_{AHE} ratio for samples in this work is 0.13–0.23, the planar Hall correction, if applied, can only change the

TABLE II. Out-of-plane HHVR results of the PMA heavy-metal/ferromagnet bilayer samples without and with the planar Hall correction versus the in-plane HHVR results on in-plane magnetized samples with similar heavy-metal resistivities and the same ferromagnetic layer. PMA results for ξ^j_{DL} are in good agreement with in-plane HHVR results only if the correction is not applied. Applying the planar Hall correction gives unrealistic numbers for the fieldlike and/or dampinglike torque efficiencies and alters the sign of the dampinglike torque of Pd(4)/Co(0.64) and the sign of both dampinglike and fieldlike torques of W(2.5)/Co-Fe-B(1). These results reveal that the planar Hall correction should be avoided in out-of-plane HHVR results.

		PMA sample without correction		PMA sample with correction		In-plane sample		
PMA sample	V_{PH}/V_{AH}	ξ^j_{DL}	ξ^j_{FL}	ξ^j_{DL}	ξ^j_{FL}	ξ^j_{DL}	ξ^j_{FL}	Ref.
W(2.2)/Co-Fe-B(1)	0.486	−0.132	−0.064	−3.52	−3.25	…	…	[35]
W(2.5)/Co-Fe-B(1)	0.54	−0.15	−0.005	0.93	1.00	…	…	[35]
Pt(4)/Co(0.75)	0.31	0.21	−0.049	0.29	0.13	0.19	−0.046	[39]
Pd(4)/Co(0.64)	0.56	0.07	−0.050	−0.1	−0.16	0.06	−0.0002	[36]
$Au_{0.25}Pt_{0.75}$(4)/Co(0.8)	0.33	0.30	−0.12	0.39	−0.14	0.32	−0.020	[40]

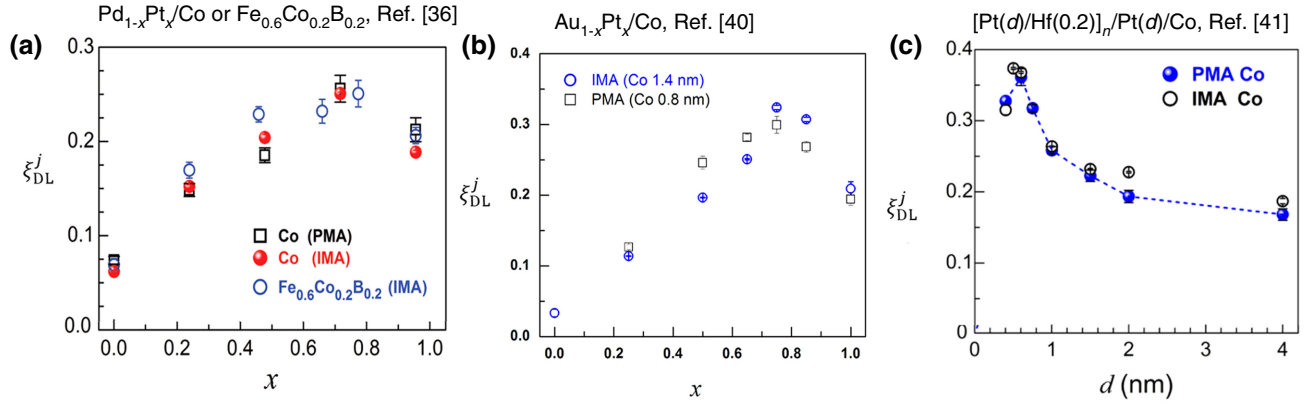

FIG. 8. Consistence of in-plane HHVR results and out-of-plane HHVR results of dampinglike spin-orbit-torque efficiencies per unit current density for (a) $Pd_{1-x}Pt_x$/(Co or $Fe_{0.6}Co_{0.2}B_{0.2}$) bilayer with different Pt concentrations in $Pd_{1-x}Pt_x$ [36], (b) $Au_{1-x}Pt_x$/Co bilayer with different Pt concentrations in $Au_{1-x}Pt_x$ [40], and (c) [Pt(d)/Hf(0.2)]$_n$/Pt(d)/Co with different thicknesses of each Pt slide [41]. "IMA" represents the in-plane harmonic Hall voltage response results from in-plane magnetized samples, while "PMA" represents the out-of-plane harmonic Hall voltage response results from perpendicular magnetic anisotropy samples, with no so-called planar Hall correction. Clearly, the out-of-plane HHVR results without planar Hall correction are reasonably close to those of the in-plane HHVR results. Note that, for most PMA samples in (a)–(c), the planar Hall correction leads to unrealistic values for the dampinglike torque efficiencies.

torque efficiencies by less than 20% and will not affect the conclusion of this work.

[1] I. M. Miron, K. Garello, G. Gaudin, P.-J. Zermatten, M. V. Costache, S. Auffret, S. Bandiera, B. Rodmacq, A. Schuhl, and P. Gambardella, Perpendicular switching of a single ferromagnetic layer induced by in-plane current injection, Nature **476**, 189 (2011).

[2] L. Liu, C. F. Pai, Y. Li, H. W. Tseng, D. C. Ralph, and R. A. Buhrman, Spin-torque switching with the giant spin Hall effect of tantalum, Science **336**, 555 (2012).

[3] L. Zhu, L. Zhu, M. Sui, D. C. Ralph, and R. A. Buhrman, Variation of the giant intrinsic spin Hall conductivity of Pt with carrier lifetime, Sci. Adv. **5**, eaav8025 (2019).

[4] L. Zhu, D. C. Ralph, and R. A. Buhrman, Maximizing spin-orbit torque generated by the spin Hall effect of Pt, Appl. Phys. Rev. **8**, 031308 (2021).

[5] Z. Chi, Y.-C. Lau, X. Xu, T. Ohkubo, K. Hono, and M. Hayashi, The spin Hall effect of Bi-Sb alloys driven by thermally excited Dirac-like electrons, Sci. Adv. **6**, eaay2324 (2020).

[6] P. N. Hai, Spin Hall effect in topological insulators, J. Magn. Soc. Jpn. **44**, 137 (2020).

[7] T.-Y. Chen, C.-W. Peng, T.-Y. Tsai, W.-B. Liao, C.-T. Wu, H.-W. Yen, and C.-F. Pai, Efficient spin–orbit torque switching with nonepitaxial chalcogenide heterostructures, ACS Appl. Mater. Interfaces **12**, 7788 (2020).

[8] L. Zhu, X. S. Zhang, D. A. Muller, D. C. Ralph, and R. A. Buhrman, Observation of strong bulk damping-like spin-orbit torque in chemically disordered ferromagnetic single layers, Adv. Funct. Mater. **30**, 2005201 (2020).

[9] Q. Liu, L. Zhu, X. S. Zhang, D. A. Muller, and D. C. Ralph, Giant bulk spin–orbit torque and efficient electrical switching in single ferrimagnetic FeTb layers with strong perpendicular magnetic anisotropy, Appl. Phys. Rev. **9**, 021402 (2022).

[10] Y. Hibino, T. Taniguchi, K. Yakushiji, A. Fukushima, H. Kubota, and S. Yuasa, Large Spin-Orbit-Torque Efficiency Generated by Spin Hall Effect in Paramagnetic Co-Ni-B Alloys, Phys. Rev. Appl. **14**, 064056 (2020).

[11] T. Nan, T. J. Anderson, J. Gibbons, K. Hwang, N. Campbell, H. Zhou, Y. Q. Dong, G. Y. Kim, D. F. Shao, T. R. Paudel, N. Reynolds, X. J. Wang, N. X. Sun, E. Y. Tsymbal, S. Y. Choi, M. S. Rzchowski, Y. B. Kim, D. C. Ralph, and C. B. Eom, Anisotropic spin-orbit torque generation in epitaxial $SrIrO_3$ by symmetry design, PNAS **116**, 16186 (2019).

[12] K. Chen and S. Zhang, Spin Pumping in the Presence of Spin-Orbit Coupling, Phys. Rev. Lett. **114**, 126602 (2015).

[13] J. Borge and I. V. Tokatly, Ballistic spin transport in the presence of interfaces with strong spin-orbit coupling, Phys. Rev. B **96**, 115445 (2017).

[14] K. Dolui and B. K. Nikolić, Spin-memory loss due to spin-orbit coupling at ferromagnet/heavy-metal interfaces: *Ab initio* spin-density matrix approach, Phys. Rev. B **96**, 220403(R) (2017).

[15] Y. Liu, Z. Yuan, R. J. H. Wesselink, A. A. Starikov, and P. J. Kelly, Interface Enhancement of Gilbert Damping from First Principles, Phys. Rev. Lett. **113**, 207202 (2014).

[16] L. Zhu, D. C. Ralph, and R. A. Buhrman, Spin-Orbit Torques in Heavy-Metal–Ferromagnet Bilayers with Varying Strengths of Interfacial Spin-Orbit Coupling, Phys. Rev. Lett. **122**, 077201 (2019).

[17] J. Bass and W. Pratt, Spin-diffusion lengths in metals and alloys, and spin-flipping at metal/metal interfaces: An experimentalist's critical review, J. Phys.: Condens. Matter **19**, 183201 (2007).

[18] J.-C. Rojas-Sánchez, N. Reyren, P. Laczkowski, W. Savero, J.-P. Attané, C. Deranlot, M. Jamet, J.-M. George, L. Vila,

and H. Jaffrès, Spin Pumping and Inverse Spin Hall Effect in Platinum: The Essential Role of Spin-Memory Loss at Metallic Interfaces, Phys. Rev. Lett. **112**, 106602 (2014).

[19] L. Zhu, D. C. Ralph, and R. A. Buhrman, Effective Spin-Mixing Conductance of Heavy-Metal–Ferromagnet Interfaces, Phys. Rev. Lett. **123**, 057203 (2019).

[20] L. Zhu, L. Zhu, and R. A. Buhrman, Fully Spin-Transparent Magnetic Interfaces Enabled by the Insertion of a Thin Paramagnetic NiO Layer, Phys. Rev. Lett. **126**, 107204 (2021).

[21] P. M. Haney, H. W. Lee, K. J. Lee, A. Manchon, and M. D. Stiles, Current induced torques and interfacial spin-orbit coupling: Semiclassical modeling, Phys. Rev. B **87**, 174411 (2013).

[22] Y.-T. Chen, S. Takahashi, H. Nakayama, M. Althammer, S. T. B. Goennenwein, E. Saitoh, and G. E. W. Bauer, Theory of spin Hall magnetoresistance, Phys. Rev. B **87**, 144411 (2013).

[23] V. P. Amin and M. D. Stiles, Spin transport at interfaces with spin-orbit coupling: Phenomenology, Phys. Rev. B **94**, 104420 (2016).

[24] L. Zhu, S. Nie, K. Meng, D. Pan, J. Zhao, and H. Zheng, Multifunctional $L1_0$-$Mn_{1.5}Ga$ films with ultrahigh coercivity, giant perpendicular magnetocrystalline anisotropy and large magnetic energy product, Adv. Mater. **24**, 4547 (2012).

[25] K. Watanabe, B. Jinnai, S. Fukami, H. Sato, and H. Ohno, Shape anisotropy revisited in single-digit nanometer magnetic tunnel junctions, Nat. Commun. **9**, 663 (2018).

[26] B. Jinnai, K. Watanabe, S. Fukami, and H. Ohno, Scaling magnetic tunnel junction down to single-digit nanometers—challenges and prospects, Appl. Phys. Lett. **116**, 160501 (2020).

[27] L. J. Zhu, D. C. Ralph, and R. A. Buhrman, Irrelevance of magnetic proximity effect to spin-orbit torques in heavy-metal/ferromagnet bilayers, Phys. Rev. B **98**, 134406 (2018).

[28] P. Sethi, S. Krishnia, S. H. Li, and W. S. Lew, Modulation of spin-orbit torque efficiency by thickness control of heavy metal layers in Co/Pt multilayers, J. Magn. Magn. Mater. **426**, 497 (2017).

[29] M. Jamali, K. Narayanapillai, X. Qiu, L. M. Loong, A. Manchon, and H. Yang, Spin-Orbit Torques in Co/Pd Multilayer Nanowires, Phys. Rev. Lett. **111**, 246602 (2013).

[30] K.-F. Huang, D.-S. Wang, H.-H. Lin, and C.-H. Lai, Engineering spin-orbit torque in Co/Pt multilayers with perpendicular magnetic anisotropy, Appl. Phys. Lett. **107**, 232407 (2015).

[31] F. Xue, S.-J. Lin, M. DC, C. Bi, X. Li, W. Tsai, and S. X. Wang, Tunable spin–orbit torque efficiency in in-plane and perpendicular magnetized $[Pt/Co]_n$ multilayer, Appl. Phys. Lett. **118**, 042405 (2021).

[32] A. Ghosh, K. Garello, C. O. Avci, M. Gabureac, and P. Gambardella, Interface-Enhanced Spin-Orbit Torques and Current-Induced Magnetization Switching of $Pd/Co/AlO_x$ Layers, Phys. Rev. Appl. **7**, 014004 (2017).

[33] H. Yang, H. Chen, M. Tang, S. Hu, and X. Qiu, Characterization of spin-orbit torque and thermoelectric effects via coherent magnetization rotation, Phys. Rev. B **102**, 024427 (2020).

[34] M. Hayashi, J. Kim, M. Yamanouchi, and H. Ohno, Quantitative characterization of the spin-orbit torque using harmonic Hall voltage measurements, Phys. Rev. B **89**, 144425 (2014).

[35] J. Torrejon, J. Kim, J. Sinha, S. Mitani, M. Hayashi, M. Yamanouchi, and H. Ohno, Interface control of the magnetic chirality in CoFeB/MgO heterostructures with heavy-metal underlayers, Nat. Commun. **5**, 4655 (2014).

[36] L. J. Zhu, K. Sobotkiewich, X. Ma, X. Li, D. C. Ralph, and R. A. Buhrman, Strong damping-like spin-orbit torque and tunable Dzyaloshinskii–Moriya interaction generated by low-resistivity $Pd_{1-x}Pt_x$ alloys, Adv. Funct. Mater. **29**, 1805822 (2019).

[37] S. Karimeddiny, T. M. Cham, D. C. Ralph, and Y. K. Luo, Sagnac interferometry for high-sensitivity optical measurements of spin-orbit torque, arXiv:2109.13759 (2021).

[38] L. Zhu and R. A. Buhrman, Absence of Significant Spin-Current Generation in Ti/Fe−Co−B Bilayers with Strong Interfacial Spin-Orbit Coupling, Phys. Rev. Appl. **15**, L031001 (2021).

[39] Y. C. Lau and M. Hayashi. Jpn. J. Appl. Phys. **56**, 0802B5 (2017).

[40] L. Zhu, D. C. Ralph, and R. A. Buhrman, Highly Efficient Spin-Current Generation by the Spin Hall Effect in $Au_{1-x}Pt_x$, Phys. Rev. Appl. **10**, 031001 (2018).

[41] L. Zhu, L. Zhu, S. Shi, M. Sui, D. C. Ralph, and R. A. Buhrman, Enhancing Spin-Orbit Torque by Strong Interfacial Scattering from Ultrathin Insertion Layers, Phys. Rev. Appl. **11**, 061004 (2019).

[42] R. J. Elliott, Theory of the effect of spin-orbit coupling on magnetic resonance in some semiconductors, Phys. Rev. **96**, 266 (1954).

[43] Y. Yafet, g factors and spin-lattice relaxation of conduction electrons, Solid State Phys. **14**, 1 (1963).

[44] L. Zhu, D. C. Ralph, and R. A. Buhrman, Enhancement of spin transparency by interfacial alloying, Phys. Rev. B **99**, 180404 (2019).

[45] L. Zhu, L. Zhu, X. Ma, X. Li, and R. A. Buhrman, Critical role of orbital hybridization in the Dzyaloshinskii-Moriya interaction of magnetic interfaces, Comm. Phys. **5**, 151 (2022).

[46] D. Weller, J. Stöhr, R. Nakajima, A. Carl, M. G. Samant, C. Chappert, R. Mégy, P. Beauvillain, P. Veillet, and G. A. Held, Microscopic Origin of Magnetic Anisotropy in Au/Co/Au Probed with X-Ray Magnetic Circular Dichroism, Phys. Rev. Lett. **75**, 3752 (1995).

[47] P. Bruno, Tight-binding approach to the orbital magnetic moment and magnetocrystalline anisotropy of transition-metal monolayers, Phys. Rev. B **39**, 865 (1989).

[48] C. Andersson, B. Sanyal, O. Eriksson, L. Nordström, O. Karis, D. Arvanitis, T. Konishi, E. Holub-Krappe, and J. Hunter Dunn, Influence of Ligand States on the Relationship between Orbital Moment and Magnetocrystalline Anisotropy, Phys. Rev. Lett. **99**, 177207 (2007).

[49] Z. Luo, Q. Zhang, Y. Xu, Y. Yang, X. Zhang, and Y. Wu, Spin-Orbit Torque in a Single Ferromagnetic Layer Induced by Surface Spin Rotation, Phys. Rev. Appl. **11**, 064021 (2019).

[50] Y. Ou, C.-F. Pai, S. Shi, D. C. Ralph, and R. A. Buhrman, Origin of fieldlike spin-orbit torques in heavy

metal/ferromagnet/oxide thin film heterostructures, Phys. Rev. B **94**, 140414(R) (2016).

[51] B. Jinnai, C. Zhang, A. Kurenkov, M. Bersweiler, H. Sato, S. Fukami, and H. Ohno, Spin-orbit torque induced magnetization switching in Co/Pt multilayers, Appl. Phys. Lett. **111**, 102402 (2017).

[52] L. Zhu, D. C. Ralph, and R. A. Buhrman, Lack of simple correlation between switching current density and spin-orbit-torque efficiency of perpendicularly magnetized spin-current-generator–ferromagnet heterostructures, Phys. Rev. Appl. **15**, 024059 (2021).

[53] L. Zhu, D. C. Ralph, and R. A. Buhrman, Unveiling the mechanism of bulk spin-orbit torques within chemically disordered Fe_xPt_{1-x} single layers, Adv. Funct. Mater. **31**, 2103898 (2021).

[54] Y. Cao, Y. Sheng, K. W. Edmonds, Y. Ji, H. Zheng, and K. Wang, Deterministic magnetization switching using lateral spin–orbit torque, Adv. Mater. **32**, 1907929 (2020).

[55] M. Tang, K. Shen, S. Xu, H. Yang, S. Hu, W. Lü, C. Li, M. Li, Z. Yuan, S. J. Pennycook, K. Xia, A. Manchon, S. Zhou, and X. Qiu, Bulk spin torque-driven perpendicular magnetization switching in $L1_0$ FePt single layer, Adv. Mater. **32**, 2002607 (2020).

[56] J. W. Lee, J. Y. Park, J. M. Yuk, and B.-G. Park, Spin-Orbit Torque in a Perpendicularly Magnetized Ferrimagnetic Tb-Co Single Layer, Phys. Rev. Appl. **13**, 044030 (2020).

[57] L. Liu, J. Yu, R. González-Hernández, C. Li, J. Deng, W. Lin, C. Zhou, T. Zhou, J. Zhou, H. Wang, R. Guo, H. Y. Yoong, G. M. Chow, X. Han, B. Dupé, J. Železný, J. Sinova, and J. Chen, Electrical switching of perpendicular magnetization in a single ferromagnetic layer, Phys. Rev. B **101**, 220402 (2020).

[58] Z. Zheng, Y. Zhang, V. Lopez-Dominguez, L. Sánchez-Tejerina, J. Shi, X. Feng, L. Chen, Z. Wang, Z. Zhang, K. Zhang, B. Hong, Y. Xu, Y. Zhang, M. Carpentieri, A. Fert, G. Finocchio, W. Zhao, and P. K. Amiri, Field-free spin-orbit torque-induced switching of perpendicular magnetization in a ferrimagnetic layer with a vertical composition gradient, Nat. Comm. **12**, 4555 (2021).